

Characteristics of a tapered undulator for the X-ray absorption fine-structure technique at PLS-II

Nark-Eon Sung, Ik-Jae Lee,* Sung-hoon Jeong and Seen-Woong Kang

Pohang Accelerator Laboratory, Pohang University of Science and Technology, Pohang 790-834, Republic of Korea. *E-mail: ijlee@postech.ac.kr

An in-vacuum undulator (IVU) with a tapered configuration was installed in the 8C nanoprobe/XAFS beamline (BL8C) of the Pohang Light Source in Korea for hard X-ray nanoprobe and X-ray absorption fine-structure (XAFS) experiments. It has been operated in planar mode for the nanoprobe experiments, while gap-scan and tapered modes have been used alternatively for XAFS experiments. To examine the features of the BL8C IVU for XAFS experiments, spectral distributions were obtained theoretically and experimentally as functions of the gap and gap taper. Beam profiles at a cross section of the X-ray beam were acquired using a slit to visualize the intensity distributions which depend on the gap, degree of tapering and harmonic energies. To demonstrate the effect of tapering around the lower limit of the third-harmonic energy, V K-edge XAFS spectra were obtained in each mode. Owing to the large X-ray intensity variation around this energy, XAFS spectra of the planar and gap-scan modes show considerable spectral distortions in comparison with the tapered mode. This indicates that the tapered mode, owing to the smooth X-ray intensity profile at the expense of the highest and most stable intensity, can be an alternative for XAFS experiments where the gap-scan mode gives a considerable intensity variation; it is also suitable for quick-XAFS scanning.

Keywords: undulator; high-order harmonic; X-ray absorption fine structure; gap-scan mode; tapered mode.

© 2014 International Union of Crystallography

1. Introduction

Synchrotron radiation from an undulator source has high brilliance and narrow spectral range (Chapman *et al.*, 1989; Kim, 1986; Attwood *et al.*, 1985; Boyanov *et al.*, 1994), and is therefore suitable for applications such as X-ray diffraction or nanoprobe/microprobe experiments. The characteristic feature of an undulator is that the spectral distribution is concentrated in a fundamental and its harmonics by interference (Kim, 1986; Alferov *et al.*, 1974; Kincaid, 1977). The 8C nanoprobe/X-ray absorption fine-structure (XAFS) beamline (BL8C) of the Pohang Light Source (PLS-II) in Korea was built for nanoprobe and XAFS experiments. The XAFS technique requires high photon flux and a spectral range as wide as 1 keV to obtain valuable spectra in regions of interest. In order to obtain a high photon flux, insertion devices, such as wigglers or undulators, have generally been used as the photon source. A wiggler has been used for the XAFS beamline because of its wide and intense spectral distribution owing to its large deflection parameter, originating from the strong magnetic field (Welter, 2012). However, because a wiggler has a stronger magnetic field in comparison with an undulator, the emittance of the storage-ring electron beam is increased such that it is higher than that of an undulator (Sasaki *et al.*, 1990).

Therefore, an undulator was chosen as the photon source for BL8C in order to minimize the emittance of the PLS-II storage-ring electron beam and to have the required brilliance for nanoprobe experiments.

Although a planar undulator (planar mode) emits brilliant X-rays, the spectral width of each harmonic is too narrow to be used in XAFS experiments. To alleviate this problem, two methods can be applied: (i) using an undulator with a gap tapering configuration whose magnetic field gradient is along the electron beam trajectory and so has a wide spectral range (tapered mode) (Boyanov *et al.*, 1994; Walker, 1988; Mori *et al.*, 2004; Barrea *et al.*, 2005; Curtin *et al.*, 1990; Hagelstein *et al.*, 1997; Fischetti *et al.*, 2004; Nonaka *et al.*, 2012; Sekizawa *et al.*, 2013; Inada *et al.*, 2007; Maréchal, 1998), and (ii) scanning the gap of a planar undulator (gap-scan mode) producing a smooth profile of the X-rays with highest intensity (Boyanov *et al.*, 1994; Mori *et al.*, 2004; Barrea *et al.*, 2005; Curtin *et al.*, 1990; Hagelstein *et al.*, 1997; Fischetti *et al.*, 2004; Nonaka *et al.*, 2012; Sekizawa *et al.*, 2013; Inada *et al.*, 2007; Maréchal, 1998; Shih & Caponi, 1982; Saitoh *et al.*, 2012; Tanaka *et al.*, 2001; Gauthier *et al.*, 1999; Rogalev *et al.*, 1998; Igarashi *et al.*, 2013; Takahashi *et al.*, 2013; Somogyi *et al.*, 2013). The gap-scan mode can be applicable to the continuous-scan (Saitoh *et al.*, 2012; Tanaka *et al.*, 2001) or high-precision step-scan

(Tanida & Ishii, 2001; Oyanagi *et al.*, 2000) by changing the undulator gap synchronized with a double-crystal monochromator (DCM) angle. On the other hand, the tapered mode is used for time-resolved experiments (Nonaka *et al.*, 2012; Tanaka *et al.*, 2001). Because the tapered mode widens the spectrum at the expense of reducing the brilliance of the undulator, a reproducible gap switch to planar mode has to be realised for nanoprobe experiments. These modes can be applied alternatively if an undulator has a tapered configuration. To realise this, a tapered in-vacuum undulator (IVU) has been installed on BL8C and operated alternatively in tapered mode and gap-scan mode for XAFS experiments.

In this paper we present the theoretical and experimental spectral distribution profiles of the incoming X-rays as a function of the gap and tapering. In addition, we discuss the effect of the IVU parameters (Table 1) on beam intensity distribution profiles and XAFS spectra in terms of gap tapering.

2. Experimental procedure

The radiation source of BL8C (Fig. 1) of PLS-II is a tapered IVU. PLS-II has been operating at 3.0 GeV and ≥ 200 mA in top-up injection mode. Synchrotron radiation from the IVU is collimated by slits and focused by a Rh-coated horizontal focusing mirror (HFM). The X-ray beam is monochromated by a Si(111) DCM, and finally delivered to the sample through a secondary source aperture. At the sample position the beam diameter is ~ 0.3 mm. A water-cooled HFM and liquid-nitrogen-cooled DCM are located at positions 20 m and 24 m from the IVU, respectively. The DCM was designed to be operated in the energy range 2.5–35.0 keV but the available energy range of the BL8C is limited to 4.0–22.0 keV due to insufficient X-ray intensity. The undulator, DCM and all devices are controlled using *Experimental Physics and Industrial Control System (EPICS)/LabVIEW* software.

When the system is operated in gap-scan mode, the gaps of the IVU are adjusted following formulae which were obtained by tracing the intensity maximums as a function of the gap and required energy. In contrast, in tapered mode, the downstream gap of the undulator was controlled in the range 0–1.2 mm

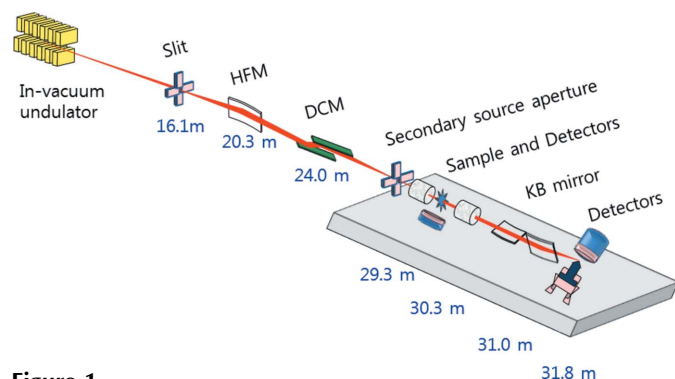


Figure 1
Schematic layout of the nanoprobe/XAFS beamline (BL8C). Positions of important optical components from the source point are shown. A nanoprobe experimental system is located downstream of the XAFS experimental set-up.

Table 1

Specifications of the in-vacuum undulator of BL8C at PLS-II. Gaps of the in-vacuum undulator are adjusted using two stepping motors with 1 μ m resolution.

Undulator type	Hybrid, asymmetric
Magnet block material	Sm ₂ Co ₁₇
Period length	20 mm
Period number	70
Undulator length	1400 mm
Working gap range	5.1–20.0 mm
Electron beam size (V \times H)	12 μ m \times 187 μ m
Electron beam divergence (V \times H)	5 μ rad \times 47 μ rad
Photon beam size (V \times H)	12 μ m \times 187 μ m
Photon beam divergence (V \times H)	49 μ rad \times 16 μ rad

with respect to the upstream gap which depends on the experimental energy range. To compare with experimental results, theoretical calculations for the tapered undulator were carried out using the *XYaup* code (Boyanov *et al.*, 1994; Sanchez del Rio & Dejus, 1998, 2004).

Beam profiles with and without tapering at energies of interest were acquired utilizing a slit located between the radiation source and HFM (Fig. 1). The slit aperture was opened to 0.1 mm \times 0.1 mm for high spatial resolution, and was raster-scanned at 0.1 mm intervals from -1.0 to 1.0 mm in the horizontal direction (x) and from -0.5 to 0.5 mm in the vertical direction (y), both with respect to the beam center. Other apertures downstream of the slit were opened enough so as not to screen the X-rays. Beam profiles and X-ray intensity distribution profiles were obtained with a nitrogen-filled ionization chamber detector. XAFS spectra were recorded at the V K -edge in planar and tapered modes to demonstrate the effect of tapering on the spectrum quality in comparison with the results of the gap-scan mode. The sample was prepared with VO₂ powder (Aldrich, 99.9%) spread thinly on a polyimide film. The incident and transmitted X-rays were monitored using two ionization chamber detectors. Because the Rh-coated HFM cannot remove contamination by high-order harmonics below 7.5 keV, X-ray intensity was detuned by more than 30% to eliminate harmonic contamination. In order to reduce spectral noise, XAFS spectra were obtained using the step-scan method.

3. Results and discussion

The IVU (Table 1) is a hybrid and asymmetric type, of length 1.4 m with 20 mm period and 140 poles. The gap range of the IVU is 5.1–20.0 mm and the available X-ray energy range is 4.0–22.0 keV. The photon beam size at the source point is 12 μ m \times 187 μ m (V \times H) and the beam divergence is 16 μ rad \times 49 μ rad (V \times H). The IVU gaps and tapering can be controlled interactively by beamline users through *EPICS*-based software to adjust the magnetic field using two stepping motors. In the case of the gap-scan mode, because the intensity of harmonics decreases significantly with increasing gap size, several formulae of the IVU gap were made using high-order harmonics with a small gap to deliver intense X-rays for all available energy ranges. On the other hand, the tapered mode needs a proper gap and tapering, depending on the energy

region, to cover an energy range of the XAFS spectrum. Beamline software recommends a proper gap formula and tapering for the gap-scan and tapered modes, respectively, depending on the operation mode.

We compared theoretical (Fig. 2a) and experimental (Fig. 2b) spectral distribution profiles of the planar mode in the energy range 4.0–20.0 keV. To show the dependency of spectral variations on undulator parameters, the gap was changed from 5.1 mm to 6.3 mm in 0.4 mm increments without tapering. Spectral features of the experimental spectra matched well with the theoretical calculations except at high energy. The first peaks correspond to the minimum energies of third-order harmonics with different gaps. Other peaks are high-order harmonics. Due to interference by the IVU radiation, peaks moved towards the high-energy side as the gap increased but the maximum intensities decreased gradually. Because the lower limit of the IVU gap is 5.1 mm (Table 1), the peak near 5.45 keV corresponds to the minimum energy of the third-harmonic X-rays. To obtain precise harmonic energies, the secondary source aperture (SSA) (Fig. 1) was located at the central spot of the radiation cone by finding the intensity maximum. Otherwise, the intensity maximum of a harmonic moved towards the lower energy side as a function of the vertical distance between the SSA and

central spot of the radiation cone, which is contrary to the report of Guo *et al.* (1999). Theoretically, even-order harmonic radiation is not included in undulator spectra for an ideal undulation. However, this was observed in Fig. 2(a) with relatively low intensity, and is ascribed to the non-zero emittance of electrons in the storage ring (Walker, 1988).

We also compared theoretical (Fig. 3a) and experimental (Fig. 3b) spectral distribution profiles of the tapered mode in the energy range 4.0–20.0 keV. To show that spectral variations depend on the undulator parameters, the gap tapering was changed from 0 to 1.2 mm in 0.4 mm increments with IVU tapering. As the degree of tapering increased, intensities decreased significantly and the spectral widths of peaks increased to form plateau shapes. Moreover, intensity plateaus moved towards the higher energy side proportional to the energy, resulting in a considerable decrease of the intensities at the peak position of zero-tapering. For the same tapering, the spectral broadness was larger at high energy than at low energy. These results indicate that a larger tapering is needed at low energy for low-order harmonics in order to have a wide spectral range but lower X-ray intensity.

To observe the intensity distribution of the IVU radiation as functions of X-ray energy and IVU parameters, X-ray beam profiles of cross sections of X-rays were obtained utilizing a

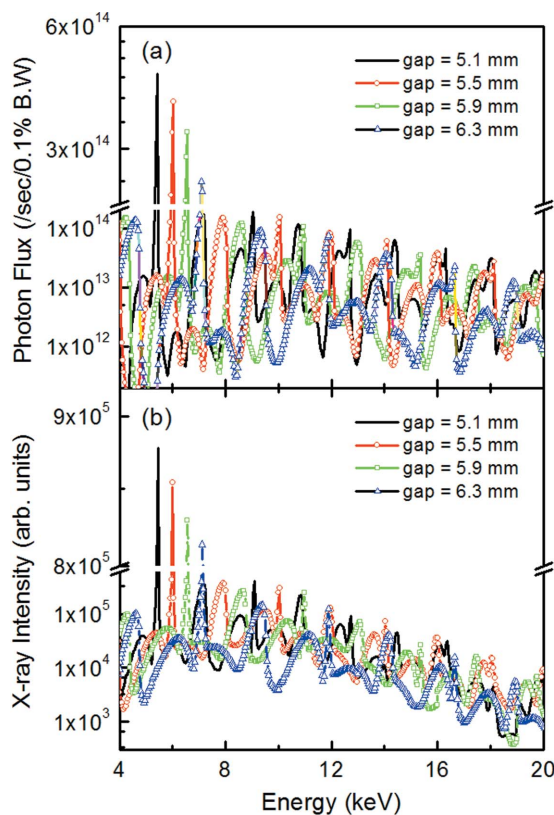


Figure 2 (a) Theoretical and (b) experimental spectral distribution profiles of the IVU in planar mode as a function of the gap with 0.4 mm intervals at 30 m from the IVU. The theoretical calculation was carried out for an electron beam of 400 mA with 3.0 GeV. Horizontal and vertical electron beam sizes of 186.6 and 12.0 μm and horizontal and vertical electron beam divergences of 46.6 and 4.8 μrad are used.

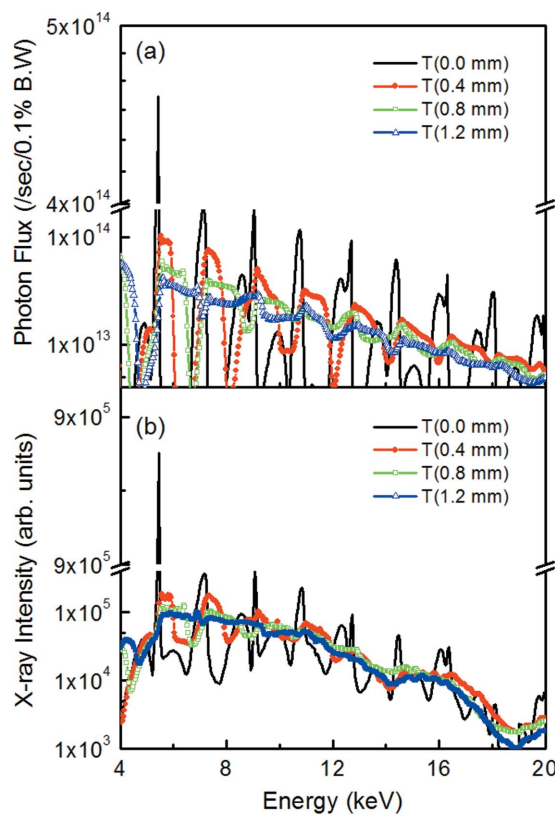


Figure 3 (a) Theoretical and (b) experimental spectral distribution profiles of the IVU in tapered mode as a function of the gap tapering with 0.4 mm interval at 30 m from the IVU. The theoretical calculation was carried out for an electron beam of 400 mA with 3.0 GeV. Horizontal and vertical electron beam sizes of 186.6 and 12.0 μm and horizontal and vertical electron beam divergences of 46.6 and 4.8 μrad are used.

slit located between the IVU and HFM (Fig. 1). Profiles of the third harmonics (Fig. 4), normalized to their maximum intensity, were obtained while keeping the gap of the IVU at 5.1 mm in planar and tapered modes at 5.45 keV [Figs. 4(a) and 4(c)] and 5.60 keV [Fig. 4(b) and 4(d)], which correspond to energies of the first maximum and minimum intensity of the third harmonics, respectively. In the planar mode the profile at 5.45 keV (Fig. 4a) shows a peak at the center with an elliptical peaked top, whereas the profile at 5.60 keV (Fig. 4c) has a valley form. In the tapered mode, the profile at 5.45 keV (Fig. 4b) has a minimum at the center contrary to Fig. 4(a), whereas the profile at 5.60 keV (Fig. 4d) has a peak at the center with a gentle slope and high intensity. These features show that intensity variation is smaller in the tapered mode than in the planar mode.

Profiles of the fourth [Figs. 5(a) and 5(b)] and fifth [Figs. 5(c) and 5(d)] harmonics with 5.1 mm IVU gap were obtained in planar and tapered modes at the first peak positions of both harmonics. In the planar mode, peaks at the center of the profiles and absolute intensities of the odd-order harmonics [Figs. 4(a) and 5(c)] were sharper and higher than that of the even-order harmonics (Fig. 5a). In contrast, profiles of tapered modes [Figs. 4(b) and 5(b)] show bowl shapes due to the blue-shift of the intensity plateaus. The profile of the fifth harmonics in tapered mode (Fig. 5d) showed higher intensity at the center than other tapered mode profiles. These results are ascribed to the fact that the intensity plateau of the tapered fourth harmonics overlap the zero-tapered fifth-order harmonic peak (Fig. 3).

The best experimental condition for XAFS experiments can be achieved using the gap-scan mode. However, because the minimum energy of the third harmonics is 5.45 keV, the XAFS spectrum in the range below 5.45 keV could be obtained in the tapered or gap-scan mode using the fundamental or second-harmonic X-rays, but the intensities of those harmonics are very low.

To demonstrate the tapering effect clearly, V *K*-edge XAFS spectra of VO₂

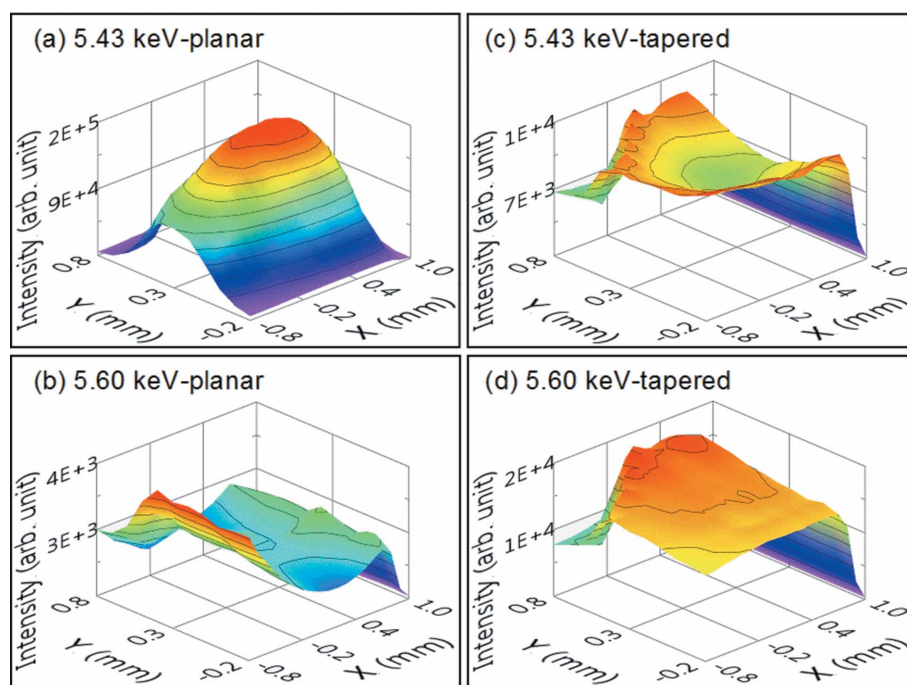


Figure 4

Beam intensity profiles, normalized to maximum intensity, at several harmonic energies were obtained while keeping the gap of the IVU at 5.1 mm (*x*, *y*: horizontal and vertical directions of the slit, respectively). Profiles in (a) and (b) were acquired at the minimum energy of the third harmonics in planar and tapered modes, respectively; those in (c) and (d) were acquired at 5.6 keV in planar and tapered modes, respectively.

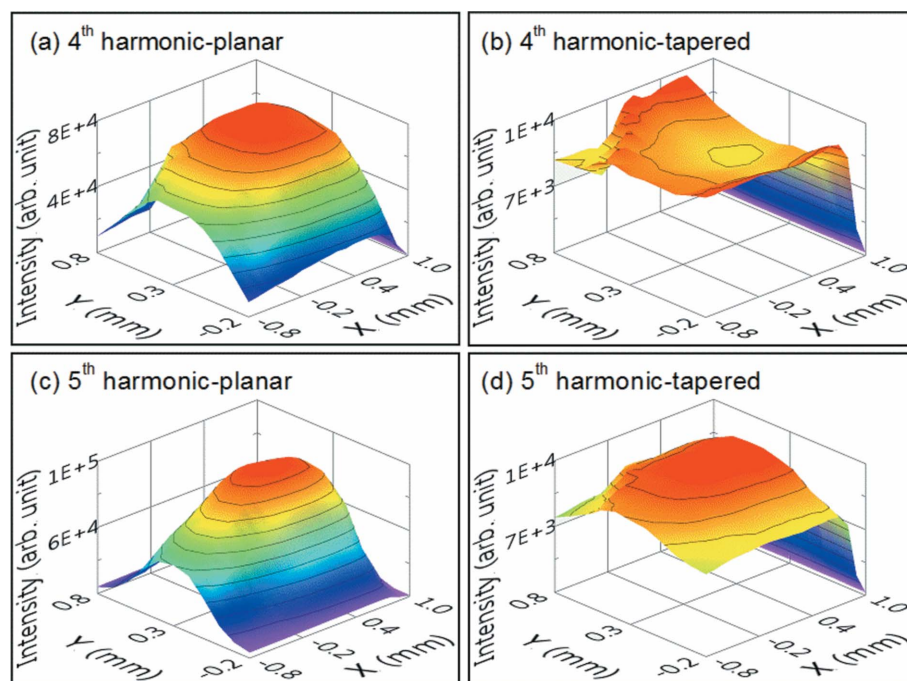


Figure 5

Beam intensity profiles, normalized to maximum intensity, at the fourth and fifth harmonic energies were obtained while keeping the gap of the IVU at 5.1 mm. Profiles in (a) and (b) were acquired at the minimum energy of the fourth harmonics in planar and tapered modes, respectively; those in (c) and (d) were acquired at the minimum energy of the fifth harmonics in planar and tapered modes, respectively.

were obtained in transmission mode in the range 5.2–6.4 keV which includes the minimum energy of the third harmonics. Although the fundamental or second harmonics give higher intensities than the third harmonics below 5.45 keV, third-harmonic X-rays were used for the gap-scan and planar modes because they give more intense X-rays than the fundamental or second harmonics above this energy. Second-harmonic X-rays were used for the tapered mode. The X-ray intensities and XAFS spectra were measured at the V *K*-edge in three operation modes with a gap of 5.1 mm. Above the minimum energy of the third harmonics (5.45 keV), the X-ray intensity (Fig. 6*a*) of the tapered mode was less than 10% of the gap-scan mode, and had intensity variations in the plateau range which were not observed clearly in the theoretical calculations. Below 5.45 keV, the X-ray intensity of the gap-scan mode was the same as that of the planar mode.

To observe variations of the X-ray intensity distribution around 5.45 keV, beam profiles were obtained. The coordinates of the beam intensity profiles in this figure are the same as used in Fig. 5. Below 5.45 keV, the beam profile shows two peaks split vertically. These peaks were merged into a single peak at 5.45 keV with increased intensity. In contrast, as the X-ray energy increased, the peak was divided into two peaks

horizontally with decreased intensity. The intensity profile was changed to a valley shape at the energy of the first intensity-minimum of the third-order harmonics. Beam profiles of below and above 5.45 keV indicate that lower- or higher-energy harmonic X-rays, in comparison with the minimum energy of the on-axis harmonics, can be obtained by selecting an off-axis peak. The energy differences between the on-axis and off-axis X-rays are given as functions of the distance between the peak and central spot of the radiation cone. Although off-axis odd-order harmonics can be applicable instead of low-intensity even-order harmonics where the energy region is below the minimum energy of the harmonics, its intensity is decreased as a function of the distance between the peak and central spot of the radiation cone.

XAFS spectra taken in planar and gap-scan modes (Fig. 6*b*) show distorted spectral features around the beginning and absorption edge (Fig. 6*b*, inset) in comparison with the spectrum of the tapered mode. These distortions are ascribed to significant intensity variations around the minimum of the third-harmonic energy accompanied with the non-linear responses of the ionization chamber detectors (Tanaka *et al.*, 2001). The distortions were reduced when the linearity was improved by reducing the X-ray intensity variation, but this reduction contradicts the purpose of securing the maximum intensity. Actually, when the BL8C IVU was used in continuous-scan or step-scan mode, the gap-scan mode gave better spectra than the tapered mode for available energy regions due to the intense X-rays. However, the tapered mode can be an alternative where the gap-scan has a considerable intensity variation and is suitable for quick-XAFS scanning.

4. Conclusion

We present the characteristic features of the BL8C IVU, operated in planar, tapered and gap-scanning modes, as a function of gap and gap tapering. The experimental spectral distributions of the IVU agree well with theoretical calculations in the range 4–20 keV. Beam intensity profiles around the energy of the intensity maximum of the third harmonic were obtained in different IVU operation modes to examine how the spectral variations depend on the IVU parameters and X-ray energies. Furthermore, XAFS spectra at the V *K*-edge were obtained to show the intensity variation and the effect of the IVU parameters on spectral quality. The XAFS spectra indicate that gap-scan mode, owing to the intense X-rays, is suitable for XAFS experiments for available energy regions when the IVU was used in continuous-scan or step-scan mode. The tapered mode, as well as being suitable for quick-XAFS scanning, can be an alternative where the gap-scan gives a considerable intensity variation.

The XAS experiments were performed with approval of authorities from the Pohang Light Source (PLS). This research was supported by the Basic Science Research Program through the National Research Foundation of Korea (NRF) funded by the Ministry of Education, Science and Technology (2011-0022268).

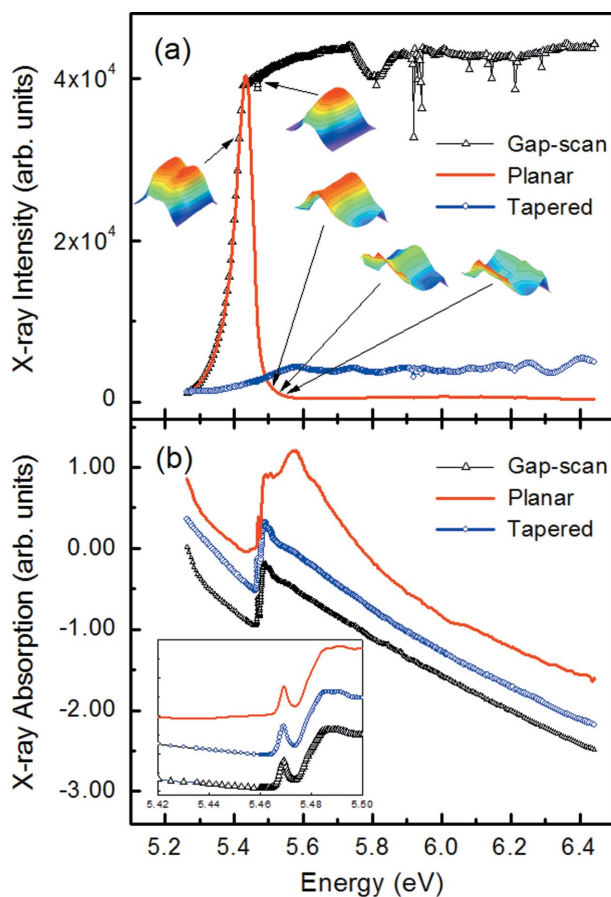


Figure 6 (a) X-ray intensities and (b) XAFS spectra at the V *K*-edge (5.439 keV) in planar, tapered and gap-scan modes with a gap of 5.1 mm. Inset: XAFS spectra around the absorption-edge region. Spectra are shifted along the y axis for a clearer view. Coordinates of beam intensity profiles are the same as in Fig. 5.

References

- Alferov, D. F., Bashmakov, Yu. A. & Bessonov, E. G. (1974). *Sov. Phys. Tech. Phys.* **18**, 1336–1339.
- Attwood, D., Halbach, K. & Kim, K. J. (1985). *Science*, **228**, 1265–1272.
- Barrea, R. A., Fischetti, R., Stepanov, S., Rosenbaum, G., Kondrashkina, E., Bunker, G. B., Black, E., Zhang, K., Gore, D., Heurich, R., Vukonich, M., Karanfil, C., Kropf, A. J., Wang, S. & Irving, T. C. (2005). *Phys. Scr.* **115**, 867–869.
- Boyanov, B. I., Bunker, G., Lee, J. M. & Morrison, T. I. (1994). *Nucl. Instrum. Methods Phys. Res. A*, **339**, 596–603.
- Chapman, K., Lai, B., Cerrina, F. & Vicarro, J. (1989). *Nucl. Instrum. Methods Phys. Res. A*, **283**, 88–99.
- Curtin, M., Bhowmik, A., Brown, J., McMullin, W., Metty, P., Benson, S. V. & Madey, J. M. J. (1990). *Nucl. Instrum. Methods Phys. Res. A*, **296**, 69–74.
- Fischetti, R., Stepanov, S., Rosenbaum, G., Barrea, R., Black, E., Gore, D., Heurich, R., Kondrashkina, E., Kropf, A. J., Wang, S., Zhang, K., Irving, T. C. & Bunker, G. B. (2004). *J. Synchrotron Rad.* **11**, 399–405.
- Gauthier, C., Solé, V. A., Signorato, R., Goulon, J. & Moguiline, E. (1999). *J. Synchrotron Rad.* **6**, 164–166.
- Guo, J.-H., Butorin, S. M., Sathe, C., Nordgren, J., Bassler, M., Feifel, R., Werin, S., Georgsson, M., Andersson, A., Jurvansuu, M., Nyholm, R. & Eriksson, M. (1999). *Nucl. Instrum. Methods Phys. Res. A*, **431**, 285–293.
- Hagelstein, M., San Miguel, A., Fontaine, A. & Goulon, J. (1997). *J. Phys. IV*, **7(C2)**, 303–308.
- Igarashi, N., Shimizu, N., Koyama, A., Mori, T., Ohta, H., Niwa, Y., Nitani, H., Abe, H., Nomura, M., Shioya, T., Tsuchiya, K. & Ito, K. (2013). *J. Phys. Conf. Ser.* **425**, 072016.
- Inada, Y., Suzuki, A., Niwa, Y. & Nomura, M. (2007). *AIP Conf. Proc.* **879**, 1230–1233.
- Kim, K.-J. (1986). *Nucl. Instrum. Methods Phys. Res. A*, **246**, 67–70.
- Kincaid, B. M. (1977). *J. Appl. Phys.* **48**, 2684.
- Maréchal, X.-M. (1998). *J. Synchrotron Rad.* **5**, 401–402.
- Mori, T., Nomura, M., Sato, M., Adachi, H., Uchida, Y., Toyoshima, A., Yamamoto, S., Tsuchiya, K., Shioya, T. & Kawata, H. (2004). *AIP Conf. Proc.* **705**, 255–258.
- Nonaka, T., Dohmae, K., Araki, T., Hayashi, Y., Hirose, Y., Uruga, T., Yamazaki, H., Mochizuki, T., Tanida, H. & Goto, S. (2012). *Rev. Sci. Instrum.* **83**, 083112.
- Oyanagi, H., Ishii, M., Lee, C.-H., Saini, N. L., Kuwahara, Y., Saito, A., Izumi, Y. & Hashimoto, H. (2000). *J. Synchrotron Rad.* **7**, 89–94.
- Rogalev, A., Gotte, V., Goulon, J., Gauthier, C., Chavanne, J. & Elleaume, P. (1998). *J. Synchrotron Rad.* **5**, 989–991.
- Saitoh, Y., Fukuda, Y., Takeda, Y., Yamagami, H., Takahashi, S., Asano, Y., Hara, T., Shirasawa, K., Takeuchi, M., Tanaka, T. & Kitamura, H. (2012). *J. Synchrotron Rad.* **19**, 388–393.
- Sanchez del Rio, M. & Dejus, R. J. (1998). *Proc. SPIE*, **3448**, 340–345.
- Sanchez del Rio, M. & Dejus, R. J. (2004). *Proc. SPIE*, **5536**, 171–174.
- Sasaki, S., Youngman, B. & Winick, H. (1990). *Nucl. Instrum. Methods Phys. Res. A*, **291**, 401–407.
- Sekizawa, O. *et al.* (2013). *J. Phys. Conf. Ser.* **430**, 012020.
- Shih, C. C. & Caponi, M. Z. (1982). *Phys. Rev. A*, **26**, 438–450.
- Somogyi, A., Kewish, C. M., Ribbens, M., Moreno, T., Polack, F., Baranton, G., Desjardins, K. & Samama, J. P. (2013). *J. Phys. Conf. Ser.* **463**, 012027.
- Takahashi, K., Imamura, M., Yamamoto, I., Azuma, J., Ogawa, K., Kamada, M., Ohkuma, H. & Yamamoto, S. (2013). *J. Phys. Conf. Ser.* **425**, 072007.
- Tanaka, T., Matsubayashi, N., Imamura, M. & Shimada, H. (2001). *J. Synchrotron Rad.* **8**, 345–347.
- Tanida, H. & Ishii, M. (2001). *Nucl. Instrum. Methods Phys. Res. A*, **467–468**, 1564–1567.
- Walker, R. P. (1988). *Nucl. Instrum. Methods Phys. Res. A*, **267**, 537–546.
- Welter, E. (2012). *J. Synchrotron Rad.* **19**, 905–910.